ACS APPLIED MATERIALS & INTERFACES

www.acsami.org

Research Article

Octahedral Molybdenum Iodide Clusters Supported on Graphene for Resistive and Optical Gas Sensing

Juan Casanova-Chafer,* Rocio Garcia-Aboal, Pedro Atienzar, Marta Feliz,* and Eduard Llobet

Cite This: *ACS Appl. Mater. Interfaces* 2022, 14, 57122−57132

Read Online

ACCESS | Metrics & More | Article Recommendations | Supporting Information

ABSTRACT: This paper reports for the first time a gas-sensitive nanohybrid based on octahedral molybdenum iodide clusters supported on graphene flakes (Mo_6@Graphene). The possibility of integrating this material into two different transducing schemes for gas sensing is proposed since the nanomaterial changes both its electrical resistivity and optical properties when exposed to gases and at room temperature. Particularly, when implemented in a chemoresistive device, the Mo_6@Graphene hybrid showed an outstanding sensing performance toward NO_2, revealing a limit of quantification of about 10 ppb and excellent response repeatability (0.9% of relative error). While the Mo_6@Graphene chemoresistor was almost insensitive to NH_3, the use of an optical transduction scheme (changes in photoluminescence) provided an outstanding detection of NH_3 even for a low loading of Mo_6. Nevertheless, the photoluminescence was not affected by the presence of NO_2. In addition, the hybrid material revealed high stability of its gas sensing properties over time and under ambient moisture. Computational chemistry calculations were performed to better understand these results, and plausible sensing mechanisms were presented accordingly. These results pave the way to develop a new generation of multi-parameter sensors in which electronic and optical interrogation techniques can be implemented simultaneously, advancing toward the realization of highly selective and orthogonal gas sensing.

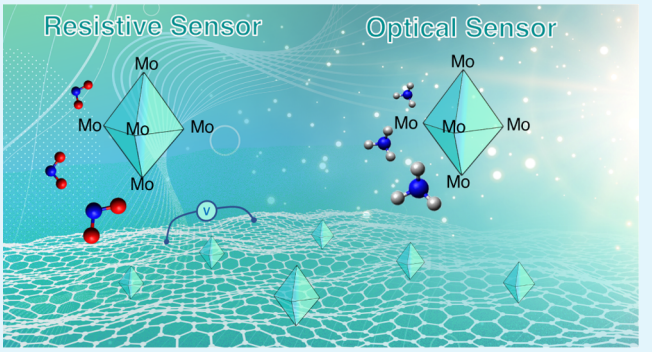

KEYWORDS: *molybdenum cluster, graphene, gas detection, resistive sensor, optical sensor*

INTRODUCTION

Air pollution is probably the largest environmental health threat worldwide, accounting for 7 million premature deaths every year.[1] Despite the fact that some techniques, such as gas chromatography coupled to mass spectroscopy, can selectively detect pollutants at trace levels, these instrumental techniques are costly, bulky, use consumables, and require frequent attention from qualified personnel. This is why automated air quality control stations are few and sparsely distributed in specific areas. However, effective pollution monitoring can only be achieved through a network of denser analysis locations (higher granularity) distributed over wider areas.[2] In other words, the ubiquitous, unattended, and real-time detection of harmful gases would protect human health by allowing the taking of pertinent actions in space and time. In this perspective, the development of gas sensors with the ability to monitor low concentrations of flammable, combustible, or toxic gases in real time is crucial. These devices should gather essential properties such as reliability, sensitivity, selectivity, repeatability, accuracy, and long-term stability together with inexpensiveness and low power consumption.

Among the different technologies for developing gas sensors, chemoresistive devices have attracted great research efforts owing to their simple driving and readout instrumentation, durability, high potential for miniaturization, and industrial scalability.[3] For decades, metal oxide (MOX) semiconductors have dominated the field of gas detection because of their high sensitivity, non-toxicity, and availability.[4] However, their poor selectivity and power-hungriness (operation temperatures are high above room temperature) are still preventing their effective implementation in commercial applications for air quality monitoring stations or unattended gas sensing networks. Therefore, the development of new and energy-efficient gas-sensitive nanomaterials is still much needed.

In recent years, carbon nanomaterial-based sensors, especially those employing graphene, have become a common approach for developing devices that operate at room temperature.[5] Room-temperature-operated gas sensors are energy efficient and help reduce fabrication costs (as no

Received: August 31, 2022
Accepted: November 30, 2022
Published: December 13, 2022

heating elements are needed), which makes them very attractive for being integrated into air quality monitoring networks. Despite the noteworthy properties of graphene, such as high surface area to volume ratios, low noise levels, high carrier density and mobility, and affordable production costs,[6] there are still some issues to be overcome. Graphene, especially in its pristine form, shows limited sensitivity and selectivity. In this sense, large research efforts have been focused on modifying or functionalizing carbon-based films for improving their sensing properties. The most direct functionalization strategies are probably the modification of graphene via plasma treatments for creating defects and replacing carbon atoms with others of different nature,[7] or the use of wet chemistry processes for the covalent or non-covalent functionalization of the graphene surface.[8] With these approaches, the sensitivity of the graphene layers is generally improved, but usually the selectivity issue remains only partially addressed, owing to the poor specificity of the atoms and functional groups present on the graphene surface. Another well-known strategy is the functionalization of graphene with organic compounds such as macrocycles, aptamers, or cavitands.[9,10] This approach significantly improves the selectivity because of the high specificity of the organic compounds (i.e., acting as chemical receptors) toward specific gases. However, the organic nature of this functionalization, which is prone to degradation under operational conditions, may compromise long-term device stability. Additionally, high specificity may result in limited reversibility of the gas−solid interactions, which compromises response repeatability. Finally, the last mainly used strategy is the decoration of graphene with metal or MOX nanoparticles.[11,12] With that, it is possible to significantly increase the sensitivity and tune the selectivity to some extent. However, these MOX nanoparticles usually need moderate or high operating temperatures for activating their sensing properties. Therefore, the achievement of low-power and inexpensive devices can be jeopardized.

As an alternative, molybdenum chalcogenides and their derivatives have been extensively explored for gas detection in the last few years.[13−15] These nanostructured semiconductors vary in composition and morphology, which impacts their sensing performance.[16,17] Besides, the fabrication of molybdenum sensors is attractive due to their abundance and low toxicity, the development of thin films and nanoparticles being the most common strategy.[18] However, there is significant scope remaining to explore new molybdenum materials with advanced properties for large-scale fabrication. Particularly, materials composed of architectured nanometer-sized octahedral molybdenum clusters (<2 nm) are very attractive for gas sensing purposes.[19] These $[Mo_6L^i_8L^a_6]$ cluster units are robust entities composed of inner halide ligands (L^i) and organic or inorganic apical (or terminal) ligands (L^a). Mo_6 clusters act as powerful photosensitizers and are also efficient luminophores that, under photoactivation, either exhibit phosphorescence in the 550−900 nm window or react with oxygen to provide singlet molecular oxygen ($^1O_2$) directed to cell damage by oxidative stress and to theranostic applications. Until now, the existing literature on analyte sensing using Mo_6 cluster-based nanomaterials encompasses optical oxygen sensors,[20−24] optical sensing of antibiotics and nitroaromatic compounds in solution,[25,26] and cluster dependence on environmental parameters, such as humidity or light.[27,28] However, Mo_6 clusters have not been applied to the detection of air pollutants until now, and the research of the materials composed of Mo_6 clusters and graphene and graphene oxide was limited to the photocatalytic field.[29−32]

To the best of our knowledge, the use of hexanuclear molybdenum cluster nanomaterials for the detection of pollutant species in the gas phase remains unexplored. Therefore, this paper encompasses, for the first time, the preparation of a Mo_6@Graphene nanohybrid composed of a crystalline octahedral molybdenum iodide cluster material supported on graphene, and the integration of this hybrid onto a transducing platform, enabling chemoresistive and optical gas sensing. The detection of two gaseous species such as nitrogen dioxide (NO_2) and ammonia (NH_3) is studied. NO_2 is an electron-withdrawing compound mainly released by automotive emissions and combustion of conventional fossil fuels, which has become a major environmental concern because it contributes to the formation of photochemical smog, acid rain, and particulate matter through chemical reactions in the atmosphere. Ammonia emissions are associated with industrial livestock, fertilizer production processes, and crop agriculture. As a highly toxic and corrosive agent, they threatenhuman health and the environment.[33] Besides reporting the sensing properties of the Mo_6@Graphene hybrid nanomaterial, its thorough morphological and compositional characterization is reported as well. Finally, the gas sensing mechanisms involved in the chemoresistive and optical detection are presented and discussed.

RESULTS AND DISCUSSION

Synthesis and Characterization of the Nanomaterials. The crystalline $[Mo_6I^i_8(OH)^a_4(H_2O)^a_2]\cdot 2H_2O$ (Mo_6) material and its derived nanohybrid (Mo_6@Graphene) were prepared and analyzed using several techniques such as Raman spectroscopy, powder X-ray diffraction, field-emission scanning electron microscopy (FESEM), and high-resolution transmission electron microscopy (HR-TEM). The synthesis of Mo_6 was achieved by the hydrolysis of $(Bu_4N)_2[Mo_6I^i_8(O_2CCH_3)^a_6]$.[29] The immobilization of Mo_6 on graphene was done by mixing the respective precursors dispersed in dichloromethane and confirmed through Raman spectroscopy (Figure S1a), resulting in Mo_6@Graphene. In this regard, the Raman shifts below 360 cm^{-1} are associated with the presence of molybdenum clusters present in the Mo_6 material (Figure S1b), while at higher frequencies, the characteristic D, G, 2D, and D′ bands of graphene appear at 1347, 1588, 2712, and 2938 cm^{-1}, respectively. The D band is associated with the presence of structural defects, disordered carbon atoms in the sp^2 configuration, and carbonaceous impurities, while the G band is related to in-plane vibrations of sp^2 carbon bonds. Thereby, the D/G ratio revealed low crystalline graphene, and the presence of defects and oxygenated functional groups grafted to the graphene is probably supporting the immobilization of molybdenum clusters. The immobilized inorganic clusters at the graphene surface are essential in gas sensing performance, enabling higher interactions with gas compounds. Furthermore, the integrity and crystallinity of the cluster-based materials after the thermal treatment (60 °C) needed for the preparation of the resulting Mo_6@Graphene were studied. Figure S1b shows intense bands with Raman shifts at 129, 153, 292, and 357 cm^{-1} associated with the Mo−Mo, Mo−I, and Mo−O vibrations of the cluster.[29,34] These Raman shifts are similar to those reported for similar hexamolybdenum clusters with iodide materials, revealing that the thermal treatment applied

https://doi.org/10.1021/acsami.2c15716
ACS Appl. Mater. Interfaces 2022, 14, 57122−57132

during the experimental protocol does not damage the cluster crystallinity owing to the lack of differences between both spectra. The suitable cluster synthesis and integrity after the thermal treatment were also confirmed through powder X-ray diffraction. Figure S2a depicts the diffractogram of the Mo_6 material, which shows a family of planes associated with a preferential orientation of the crystalline material upon deposition onto the glass surface.[29] The Mo_6 crystallinity was preserved after the thermal process applied during the deposition step (Figure S2b). Figure S2c shows the diffractogram of the Mo_6@Graphene after the deposition process. Considering the low graphene crystallinity, it is noteworthy that some intense peaks associated with the crystallinity of Mo_6 can be noticed in the nanohybrid, evidencing the presence of supported cluster crystals. Thereby, the X-ray diffraction also confirms that the synthesis and deposition processes developed avoided the degradation of molybdenum cluster-based material. The robustness of the prepared cluster materials is an advantage for preparing gas sensors and conducting the resistive and optical measurements described below. Regarding the binding interaction between the crystalline cluster phase and the graphene sheets, we think that it could mainly be associated with supramolecular interactions, such as Van der Waals and charge electrostatic and polar interactions, due to the polarity induced by the cluster units and the presence of water molecules embedded into the hydrogen-bonded network of the crystalline cluster phase and the preference of such water molecules to adsorb on residual defects and sites with oxygen-containing functional groups.[30,35,36] However, the cluster immobilization of $\{Mo_6I^i_8\}^{4+}$ cluster cores through coordinative bonds to such oxygen functionalities, as occurs with GO, cannot be discarded.[29] Additional research on the study of the binding interactions involved is under current investigation.

Finally, the resulting Mo_6@Graphene nanomaterial was analyzed by FESEM and HR-TEM techniques. Figure 1a shows the graphene surface once it was deposited. A highly porous surface can be noticed (BET area of 730 m^2/g according to previous results[37]), which can be interesting from the sensing point of view. Moreover, Figure 1b confirms the well-dispersed crystalline cluster particles supported on graphene. This image was taken employing a back-scattered electron (BSE) detection; consequently, bright spots correspond to Mo_6 and the dark background corresponds to graphene. HR-TEM and energy-dispersive X-ray spectroscopy (EDS) analyses of the nanomaterial confirm the presence of the $Mo_6I^i_8$ cluster units deposited onto graphene layers (Figure S3).

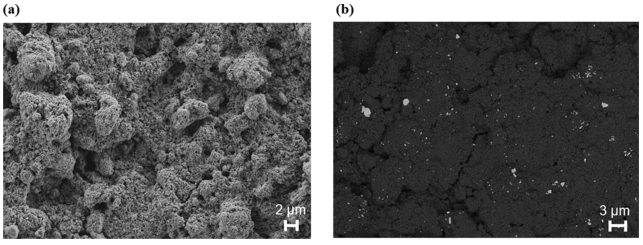

Figure 1. (a) FESEM image showing the sensor surface of bare graphene. (b) FESEM image recorded with the BSE detector of the Mo_6@Graphene material. The $\{Mo_6I^i_8\}^{4+}$ cluster core material (bright spots) supported on graphene (dark background) can be observed, revealing a suitable cluster distribution.

Gas Detection Using a Chemoresistive Transducing Scheme. The ability of the Mo_6@Graphene layer for detecting several gas species was evaluated under room temperature operation conditions. This approach leads to low power-consumption devices and reduced fabrication costs. Different concentrations (250, 500, 750, and 1000 ppb) of NO_2 were applied during several consecutive measurement cycles (Figure 2a), obtaining significant differences when graphene is loaded with molybdenum clusters in comparison to its bare counterpart (Figure S4). Specifically, the calibration curves (Figure 2b) revealed that the Mo_6@Graphene sample presents up to fivefold higher electrical responses (i.e., the intensity of the resistance changes induced by the exposure to NO_2) than bare graphene. Regarding the sensitivity, which is given by the slope of the curves shown in Figure 2b, the Mo_6@Graphene layer shows 4 times higher sensitivity toward NO_2 than bare graphene.

Considering the requirements for ambient monitoring purposes, the detection of lower NO_2 concentrations is needed, and the effect of the relative humidity should also be assessed owing to its significant effect on sensing performance. Thereby, according to the threshold limit values (TLV) defined by the Clean Air Act Text (the United States Environmental Protection Agency) and the Ambient Air Quality (European Union),[38,39] lower NO_2 concentrations ranging from 50 to 250 ppb were tested. Figure 3a shows an intelligible and repeatable detection of the target gas by the Mo_6@Graphene layer, enabling its potential use in commercial applications. It is worth noting that, even at this low range of NO_2 concentrations, the Mo_6@Graphene sensor shows good baseline stability under room temperature operation conditions. Conversely, bare graphene presents a poor sensing performance at this concentration range (Figure S5a), experiencing low repeatability due to the slight resistance changes induced by the exposure to the target gas.

Not limited to this, since ambient moisture is a well-known interfering element on the gas sensing performance,[40] NO_2 ranging from 50 to 250 ppb was also tested under humid conditions (Figure S5b). In consequence, the previous experiment carried out under dry conditions was reproduced at 60% relative humidity for the cluster-loaded graphene. Figure 3b depicts a comparison for the Mo_6@Graphene sample in both environments, revealing a significant increase in the sensing response (up to 2-fold) when the sensor is operated under humid conditions. However, the sensitivity (i.e., the slope of the calibration curve) remains almost unchanged under dry or humid conditions, which is an outstanding result toward implementation in ambient monitoring devices.

In view of the intelligible sensing responses and the low noise levels registered, the limits of detection and quantification (LOD and LOQ, respectively) were evaluated measuring trace levels of NO_2 ranging from 10 to 25 ppb (Figure S6a). The calibration curve (Figure S6b) was used for estimating both parameters through the following equations

$$\mathrm{LOQ} = 10\frac{S_y}{b} \quad LOD = 3\frac{S_y}{b}$$

where S_y are the standard deviations of y-residuals, and b corresponds to the sensitivity (slope) of the calibration curve. Besides, a factor of 10 and 3 is applied to the LOQ and LOD, respectively. As a result, the Mo_6@Graphene sensitive layer reveals a LOQ of 10.3 ppb, while the estimated LOD is 3.1

https://doi.org/10.1021/acsami.2c15716
ACS Appl. Mater. Interfaces 2022, 14, 57122−57132

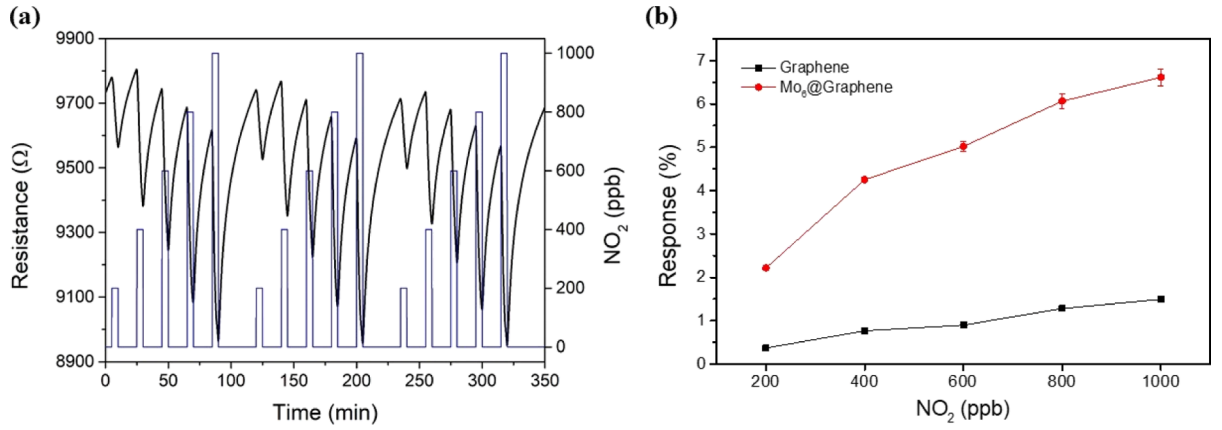

Figure 2. (a) Electrical responses toward NO_2 (range 250−1000 ppb) under room temperature operation using the Mo_6@Graphene nanomaterial. (Resistance: black line and left *y*-axis; gas concentration: blue line and right *y*-axis). (b) Comparison of the calibration curves obtained for bare graphene and Mo_6@Graphene for detecting NO_2.

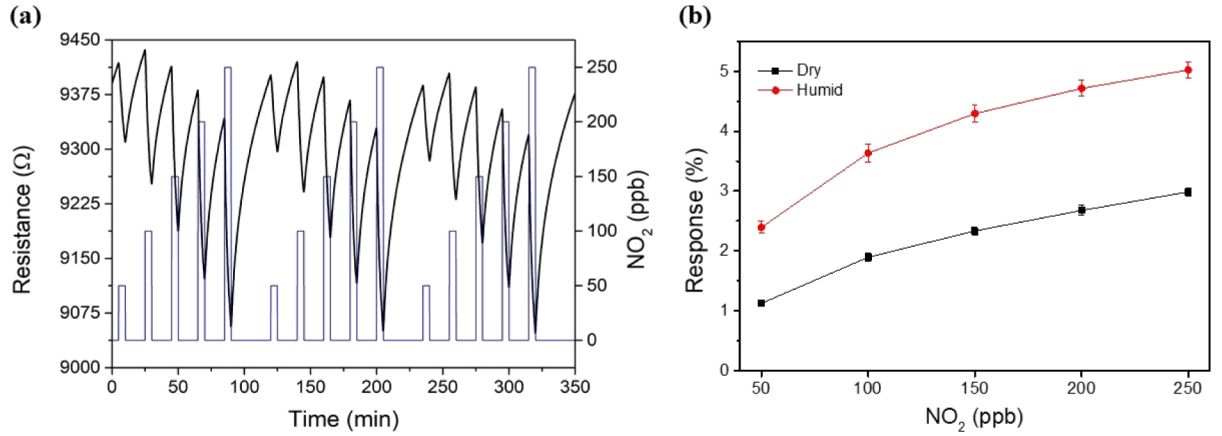

Figure 3. (a) Dynamic response toward NO_2 (range 50−250 ppb) under room temperature operation for the Mo_6@Graphene nanocomposite. (Resistance: black line and left *y*-axis; Gas concentration: blue line and right *y*-axis). (b) Comparison of the calibration curves for the Mo_6@Graphene layer in a dry and humid atmosphere.

ppb. It is worth noting that these values are far below the TLV needed for ambient monitoring applications, and the detection times are enough for enabling a reliable detection considering that the exposure limits are usually defined as the average concentrations for 8 h. The device operating conditions (i.e., 5 min of gas exposure and room temperature working conditions) result in advantageous features such as low power consumption, high sensitivity, and fast detection of gas species.

Gas sensor repeatability is a key influencing parameter that determines the potential of the developed cluster-graphene layer for being employed in gas sensing. In consequence, successive cycles of 5 min of NO_2 exposure followed by 15 min of recovery in dry air were recorded (Figure 4). As a result, the hybrid Mo_6@Graphene revealed outstanding sensor repeatability, showing an error of about 0.9%.

Apart from the detection of an electron-withdrawing gas like NO_2, the sensing performance of bare and cluster-loaded graphene was also evaluated toward an electron-donor species as ammonia (NH_3). Figure 5a shows the resistance changes obtained for the Mo_6@Graphene sample when detecting NH_3 in the range of 25−100 ppm. A significant baseline drift can be observed, probably because the sensor surface is not fully cleaned and some NH_3 is still adsorbed. This behavior is relatively frequent when gas sensors are operated at room

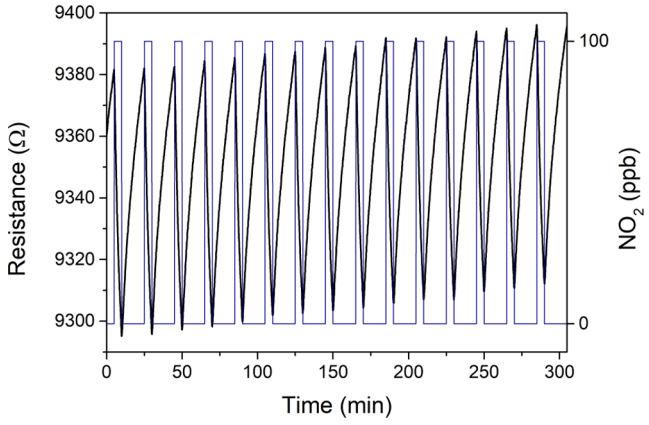

Figure 4. Repeatability experiment for the Mo_6@Graphene device by applying 15 pulses of 100 ppb of NO_2. (Resistance: black line and left *y*-axis; Gas concentration: blue line and right *y*-axis).

temperature and under low flow rates. Nevertheless, baseline drift might be ameliorated by irradiating the surface with UV light or slightly increasing the operating temperature, only to cite some strategies. Indeed, the chemoresistive response for bare graphene (Figure S7) is higher than that of cluster-loaded graphene, as Figure 5b depicts. Nevertheless, considering that

https://doi.org/10.1021/acsami.2c15716
ACS Appl. Mater. Interfaces 2022, 14, 57122−57132

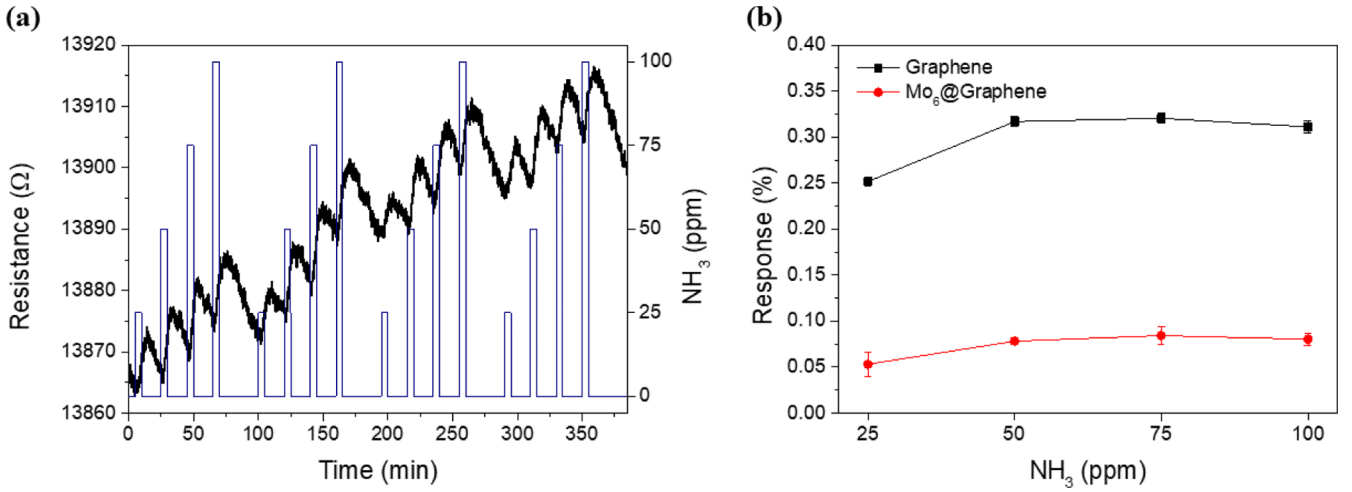

Figure 5. (a) Example of the dynamic responses for the Mo_6@Graphene sensor when detecting NH_3 under room temperature conditions. (Resistance: black line and left *y*-axis; Gas concentration: blue line and right *y*-axis). (b) Comparison of the calibration curves obtained for bare graphene and Mo_6@Graphene for detecting NH_3.

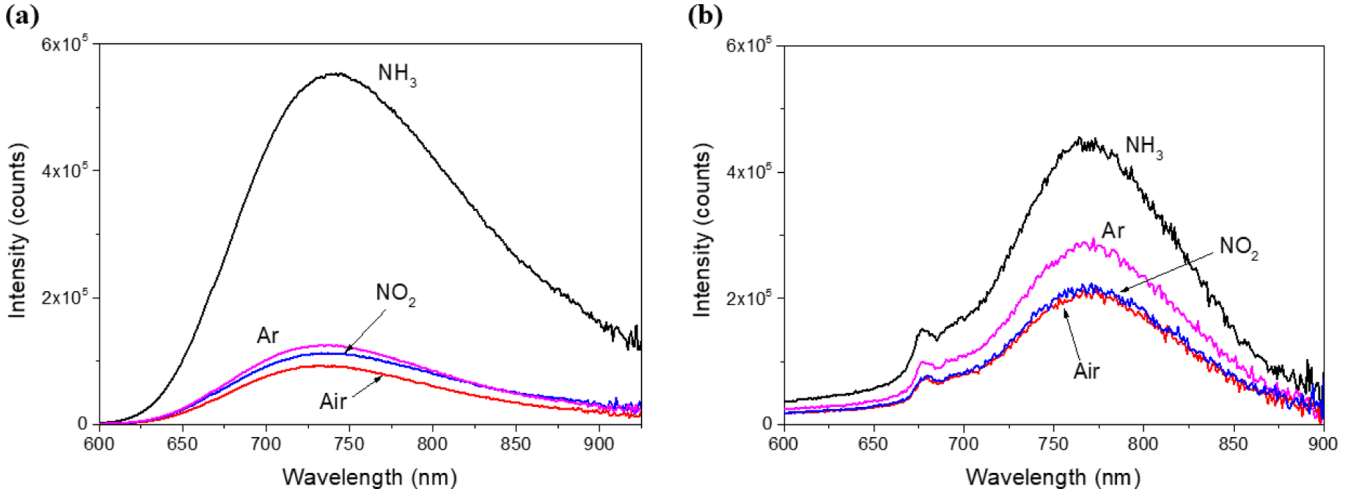

Figure 6. (a) Room-temperature PL spectra of a thin film of pure Mo_6 material deposited in a quartz substrate (λ_{ex} = 320 nm) and exposed under Ar, air, NO_2, and NH_3 gases. (b) Room-temperature PL spectra measured directly onto Mo_6@Graphene coating on the alumina substrate (λ_{ex} = 320 nm), employed in chemoresistive transduction, and exposed under Ar, air, NO_2, and NH_3 gases.

sensitivity is given by the slope of the calibration curve, it can be concluded that Mo_6@Graphene is virtually insensitive to NH_3; since responses are lower than 0.1%, these barely change when exposed to different ammonia concentrations. It should be mentioned that NH_3 sensing performance might be improved to some extent, but the same experimental conditions were applied as NO_2 for an effective comparison.

In view of these results, it was necessary to check whether or not the absence of a chemoresistive response for ammonia could be due to the decomposition of $\{Mo_6I^i_8\}^{4+}$ cluster cores, owing to the basicity of NH_3.[41] In this perspective, the Mo_6 and Mo_6@Graphene robustness upon exposure to NO_2 and NH_3 gases was evaluated by powder X-ray diffraction and Raman analyses. Figure S8 shows X-ray diffractograms for both samples before and after being exposed to the target gases. Since no change in the spectra is observed, the gas exposure does not damage the cluster crystallinity. Accordingly, the Raman spectra confirm that the cluster units are not decomposed after exposure to gases (Figure S9). This reveals the outstanding stability of the molybdenum cluster units, which are not degraded when exposed to ammonia or nitrogen dioxide.

Gas Detection Using an Optical Transducing Scheme. The optical gas sensing properties of the Mo_6@Graphene and Mo_6 materials were preliminarily investigated using films deposited on alumina and quartz transducer substrates, respectively, and in the presence of NO_2 (1 ppm) and NH_3 (250 ppm) balanced in air. Photoluminescence (PL) spectroscopy provides information about the interaction between molybdenum clusters and target gases. The steady-state emission spectrum of the pure Mo_6 crystalline material presents a broad emission band centered at 725 nm when registered under an argon atmosphere (Figure 6a). This wavelength is characteristic of the electronic triplet excited state of the$\{Mo_6I^i_8\}^{4+}$ cluster core.[42−46] A similar spectrum was registered for the Mo_6@Graphene device under an inert atmosphere (Figure 6b), but a redshift to 770 nm was detected with no interference of the characteristic emission band of graphene (Figure S10). This shift of the PL for the Mo_6@Graphene material corresponds to a band gap decrease of 0.1 eV, and it can be attributed to two main factors: the polarity

https://doi.org/10.1021/acsami.2c15716
ACS Appl. Mater. Interfaces 2022, 14, 57122−57132

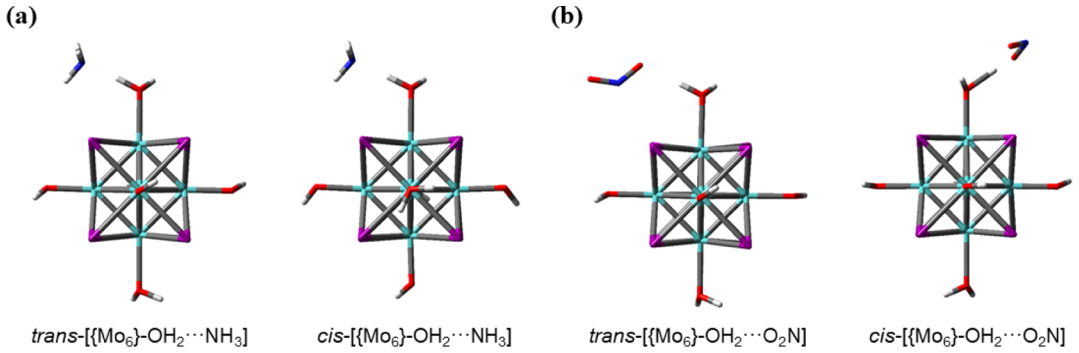

Figure 7. Representation of the most stable cluster···NH_3 (a) and cluster···NO_2 (b) models, encompassing *trans*- and *cis*-$[Mo_6I^i_8(OH)^a_4(H_2O)^a_2]$ configurations (right and left representations, respectively).

conferred by the graphene environment and the interactions between defective graphene and Mo_6 material. Both films were exposed to NO_2, NH_3, or O_2 (air) gases, and the PL changes were measured. In their in situ optical characterization, intensity variations were observed in the emission spectra with respect to the analyte gases. A decrease in the PL was observed in the presence of air with respect to exposure under argon. This is due to efficient PL quenching by oxygen, leading to the formation of singlet molecular oxygen ($^1O_2$), which is an intrinsic property of the $\{Mo_6I^i_8\}^{4+}$ cluster core materials.[47] A decrease in the PL was also observed after exposure to NO_2, and this PL quenching is achieved to a lesser extent than in the presence of air. In contrast, a high PL was detected in the presence of ammonia. The different optical responses of the molybdenum crystalline material with the NH_3 and NO_2 gases follow the same trend for the Mo_6@Graphene nanomaterial. The PL was recorded after two consecutive NH_3/Ar cycles, and the results indicated the reversibility of the PL responses (Figure S11). These surprising results indicate that "wake-up" ammonia detection of the cluster-based Mo_6 and Mo_6@Graphene materials is achieved. Apart from the donor/acceptor properties of the gas molecules, these phenomena could be associated with a strong interaction between NH_3 and the molybdenum clusters. Whereas the Mo_6 material shows high sensing performance and selectivity toward ammonia detection, only the hybrid material shows a selective double transduction scheme (optic and chemoresistive). In addition, a remarkable PL response for the Mo_6@Graphene hybrid was obtained considering the low concentration of supported clusters. A possible quenching effect of the graphene support can also be responsible for the lower selectivity toward gas analytes.[30] The stability of the Mo_6 and Mo_6@Graphene materials when exposed to ammonia or nitrogen dioxide supports the reliability of the PL spectra. Since the emission bands are exclusively associated with the luminescence of the octahedral Mo clusters, the viability of both nanomaterials as optical and chemoresistive sensors was confirmed.

Orthogonal Sensing Mechanisms. The above results show that the Mo_6@Graphene film coating over standard substrates can be interrogated using two different transducing schemes, chemoresistive and optical, for the detection of nitrogen dioxide and ammonia, respectively. This behavior would correspond to orthogonal sensing, which is a term coined in the context of detecting different toxic gases or even multi-component gas mixtures using sensor arrays. Ideally, orthogonal sensing would be achieved because at least one highly specific sensor is present in the array for every target species. In a real application, orthogonality can be achieved either by modifying/optimizing the gas-sensitive film to make it more specific to its target species (in this approach, specificity or selectivity are in general improved to a limited extent) or by constructing orthogonal metasensors built upon the combination of response features from an array of sensors with partially overlapped selectivity.[48,49] The resistive and optical results described in this work pave the way for devising a non-conventional strategy for achieving orthogonal sensing.

The factor responsible for this orthogonal behavior is related to the interaction between the target gas analytes and the molybdenum cluster-based material. The integrity of the Mo_6@Graphene and Mo_6 materials after the exposure to gases confirms that, even considering the coordinative ability of ammonia, no ligand exchange over the $\{Mo_6I^i_8\}^{4+}$ cluster units was achieved. This suggests that the gas−solid interaction would take place by other kinds of supramolecular interactions, hydrogen bonding being the most plausible one. In the case of transition metal luminophores, the hydrogen bonding interactions with polar ligands, which act as receptor sites capable to form hydrogen bonds with the target molecule, can provide changes in their characteristic luminescence response.[50−54] Since the X-ray diffraction planes of the deposited Mo_6 material suggest that the $[Mo_6I^i_8(OH)^a_4(H_2O)^a_2]$ cluster sites are preferentially exposed to gas adsorption, the sensing is probably promoted by hydrogen bonding between the apical cluster ligand (hydroxo or water) and the gaseous analytes. To reveal the interactions between the $[Mo_6I^i_8(OH)^a_4(H_2O)^a_2]$ clusters and target molecules, DFT calculations were performed using the BPE0 functional because of its robustness and excellent performance for treating hydrogen bonds.[55,56] Two stereoisomers, namely *trans* and *cis*-$[Mo_6I^i_8(OH)^a_4(H_2O)^a_2]$, were built as representative models for adsorption sites, and the reliability of this functional was confirmed by the analysis of the computed geometries of the isomers, which shows a good fit to the X-ray diffraction structure (Figure S12). The energetic interactions between the cluster compound and the gas molecules were studied by computing the binding energies (BEs) associated with the formation of a cluster-gas molecule (NH_3 or NO_2) adduct in a 1:1 ratio. In all the adducts, the gas interacts directly with water and hydroxo ligands (Figures 7 and S13) by hydrogen bonding in most cases, with BEs in good agreement to H-bonding energies (Table S1). Figure 7 illustrates the most energetically stable cluster-adduct models with the highest BEs, namely *ca.* −18 and −7 kcal/mol, associated with the isomers with H_2N···HOH and NO_2···HOH interactions, respectively. The gas-

https://doi.org/10.1021/acsami.2c15716
ACS Appl. Mater. Interfaces 2022, 14, 57122−57132

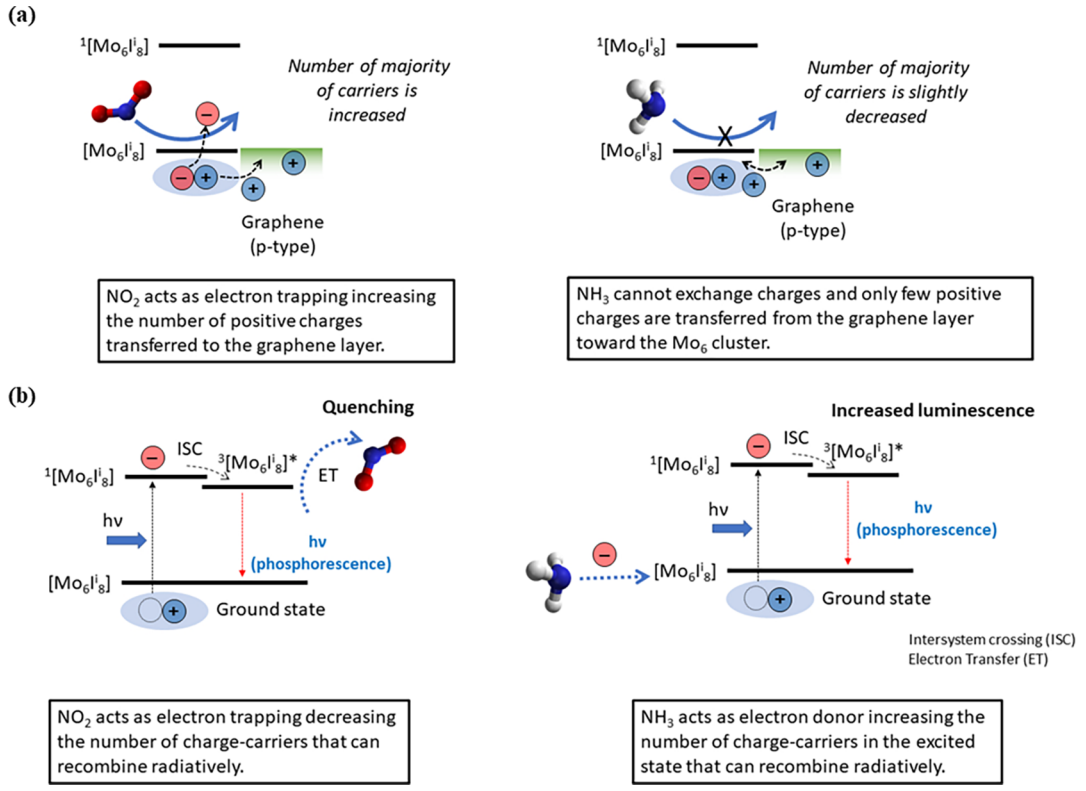

Figure 8. Schematic representation of the two sensing mechanisms proposed under resistive (a) and optical (b) conditions. The graphs on the left and right correspond to NO_2 and NH_3 gas exposure, respectively.

cluster adducts become energetically more unstable when the hydroxo ligand is involved (Table S1). In all cases, BEs are negative, indicating that the formation of cluster-gas molecule adducts is exothermic. Thus, NH_3 and NO_2 molecules are likely to be adsorbed onto the surface of the cluster-based crystalline material.

A tentative description of the sensing mechanism of $[Mo_6I^i_8(OH)^a_4(H_2O)^a_2]$ toward NH_3 and NO_2 under resistive and optical conditions is represented in Figure 8. Under resistive conditions (Figure 8a), the exposure of the molybdenum clusters to the electron-acceptor NO_2 would favor the increase of positive charges in graphene layers, resulting in a major chemoresistive response. In the presence of NH_3, its electron donor ability practically does not influence the electronic characteristics of the clusters, and, as a consequence, they would remain intact to exchange charges with graphene. This could be associated with the difficulty in the reduction of the $\{Mo_6I^i_8\}^{4+}$ cluster core compounds, considering their intrinsic redox properties.[57] One question remains open regarding the small chemoresistive response of Mo_6@graphene in the presence of ammonia in comparison with one of the bare graphenes (Figure 5). Probably, this behavior can be explained considering the close alignment of the energy bands between the fundamental state of the octahedral molybdenum clusters and the work function of graphene. The value of the work function of graphene is dependent on the oxygen functionalities (between 4.2 (pristine graphene) and 6.7 eV),[58] and the functionalization onto the graphene surface.[59] The positioning of the fundamental state of $\{Mo_6I^i_8\}^{4+}$ cluster core compounds (*ca.* 5.0−5.5 eV)[29,30] would promote the transfer of some holes from the graphene layer to the metallic cluster and concomitant compensation of charges, giving rise to a diminution of the resistive response.

Under light irradiation conditions (Figure 8b), the exposure to NH_3 gas molecules, which act as electron donors, would increase the concentration of charges in the fundamental state of $\{Mo_6I^i_8\}^{4+}$ cluster core molecules, and a huge increase in the PL intensity is detected. In contrast, the interaction of the electron acceptor NO_2 molecules with the molybdenum clusters would only slightly quench the PL in an electron transfer process, similar to that described for O_2. Probably, these photophysical effects can explain the orthogonal behavior of the Mo_6@Graphene sensor under electrical conditions. The great PL increase in the presence of NH_3 gas could promote charge recombination by emitting light and hinder charge transfer with graphene, resulting in poor resistive changes. However, the electronic structure of molybdenum clusters is practically unaffected under NO_2 gas and remains intact to exchange charges with graphene.

CONCLUSIONS

A novel nanomaterial based on molybdenum iodine clusters supported on graphene was implemented in a single gas sensing device, which employs two transduction schemes, that is, chemoresistive and optical. Noteworthily, the developed hybrid nanomaterial can work under room temperature conditions and can be easily integrated into miniaturized devices. Additionally, the crystalline material based on $\{Mo_6I^i_8\}^{4+}$ cluster cores integrated into graphene layers showed outstanding stability and low cross-sensitivity to ambient moisture. This approach has enabled the orthogonal detection of two gaseous species (i.e., NO_2 and NH_3) since nitrogen dioxide induces a chemoresistive response and not a PL response, while ammonia induces a PL response and not a chemoresistive response. DFT calculations confirmed that the

https://doi.org/10.1021/acsami.2c15716
ACS Appl. Mater. Interfaces 2022, 14, 57122−57132

gas sensing mechanisms are based on hydrogen bonding interactions between the analyte and the apical cluster water ligands of the octahedral cluster entities. Different mechanisms of charge transfer between $\{Mo_6I^i_8\}^{4+}$ cluster core molecules and the gas molecules are proposed for elucidating the chemoresistive response. The changes in the cluster emission are attributed to a change in the energy transfer efficiencies promoted by hydrogen bonding between the apical cluster ligands and NH_3. These proof-of-concept results pave the way for developing new, highly selective, and multi-parameter gas sensors by combining electronic and optical transduction schemes in a single device. In consequence, Mo_6@Graphene sensors represent an interesting alternative for achieving widespread air quality monitoring systems owing to their ease of use, inexpensiveness, low energy consumption, and outstanding gas sensing properties.

MATERIALS AND METHODS

Synthesis of $[Mo_6I^i_8(OH)^a_4(H_2O)^a_2]\cdot 2H_2O$ (Mo_6). The synthesis of Mo_6 microcrystals was achieved by optimizing a described procedure[29] from the cluster precursor $(Bu_4N)_2[Mo_6I^i_8(O_2CCH_3)^a_6]$. This was prepared by properly adapting the synthetic procedures reported in the literature from the $(Bu_4N)_2[Mo_6I^i_8I^a_6]$ and silver acetate materials.[44,60,61] In a typical procedure for preparation of Mo_6, the cluster precursor (30 mg) was dispersed in a mixture (15 mL) of water, acetone, and triethylamine in 50/45/5% v/v, respectively, in a round-bottom flask with continuous magnetic stirring (500 rpm) at room temperature. Afterward, a bubbler was connected to the flask, and the resulting yellow-orange suspension was heated to 35 °C for 1 h. Over time, the mixture evolved to a solution, which was added into a 10 mL vial sealed with a holey parafilm for its slow evaporation for 5−7 days. Finally, red microcrystals were collected from the remaining solution. The crystalline material was washed twice with acetone and once with Milli-Q water (10 mL). Notably, the optimum crystal size is achieved when the solution becomes transparent.

Mo_6@Graphene Development and Sensing Device Fabrication. For supporting the molybdenum clusters on graphene, two solutions were prepared in parallel. First, a 10 mL graphene suspension (0.5 mg/mL) in dichloromethane was performed employing graphene nanoplatelet aggregates (submicron particles, surface area 750 m^2/g, Strem Chemicals Inc., USA). Then, the resulting suspension was placed in an ultrasonic tip for achieving a proper graphene exfoliation. Particularly, a pulsed sonication (1s on/2s off) at 280 W for 90 min was applied. A 1 mL suspension of Mo_6 (0.25 mg/mL) in dichloromethane was prepared by sonication for 30 min in an ultrasonic bath. Afterward, the Mo_6 mixture was added to the graphene suspension, resulting in graphene loaded with a 5% wt of the Mo_6 cluster. The mixture was homogenized for 10 min under stirring. Subsequently, the solution was sonicated in an ultrasonic bath for 1 h, resulting in a suitable distribution of molybdenum clusters supported on graphene (Mo_6@Graphene). For the characterization of the nanomaterial, the resulting suspension was deposited onto appropriate wafers directed to each characterization technique and placed onto a hotplate at a moderate temperature (60 °C). For sensing studies, the suspension was deposited via spray coating on alumina substrates comprising platinum screen-printed electrodes (Figure S14). First, the substrates were placed onto a hotplate at a moderate temperature (60 °C), and then, the deposition process was started after few minutes for ensuring the correct heating up of the substrate. The spray coating deposition was performed using nitrogen as the carrier gas for about 45 s. As a result, homogeneous sensitive films were obtained with an average thickness of 1 μm (see cross-section, FESEM (Figure S15) and optical profilometer measurement (Figure S16)).

Characterization Techniques. UV−vis spectra were acquired at 20 °C, employing a Varian Cary 50 Conc spectrophotometer equipped with 10 × 10 mm quartz cells. Steady-state PL measurements were recorded in an Edinburgh Instruments FLS1100 spectrofluorometer using a 450 W xenon lamp light equipped with a double monochromator for excitation and emission coupled to a cooled photomultiplier (PMT-980). The Raman spectra were obtained from solid samples previously deposited onto quartz substrates using a "Reflex" Renishaw spectrometer equipped with an Olympus microscope. The exciting wavelength was 514 nm of an Ar^+ ion laser, while the laser power was ∼10−25 mW; 20 acquisitions were taken for each spectrum. Powder X-ray diffraction patterns were obtained by using a Philips X'Pert diffractometer and copper radiation (CuKα = 1.541178 Å). FESEM images were recorded with a Zeiss Ultra 55 field FESEM apparatus (Atlanta, GA, USA) equipped with a BSE detector. Samples for HR-TEM were deposited onto carbon-coated copper grids. HR-TEM images were recorded by using a JEOL JEM2100F microscope operating at 200 kV. The molybdenum and iodine contents of the Mo_6@Graphene sample were determined by dark-field scanning transmission electron microscopy (STEM) EDS analysis conducted by using an EDAX system (Oxford Instruments) attached to a JEOL JEM2100F electronic microscope. The thickness of the film was measured with a MicroXAM-100 3D surface profilometer. The cross-section was examined by FESEM (Zeiss Ultra 55 instrument).

Resistive Gas Sensing Measurements. Once homogeneous layers were achieved (Figure S14), the gas sensors were placed in an airtight testing chamber (dead volume of 35 cm^3). The chamber was subsequently connected to a gas mixing and delivery system comprising different calibrated gas cylinders. A pure dry air atmosphere (air premier purity: 99.999%) was employed during the sensing test and used as a carrier gas for the target gases. It is worth highlighting that a residual amount of relative humidity (3−4%) is present in dry conditions. The overall flow was adjusted at a low rate (100 mL/min) using a set of mass-flow controllers (Bronkhorst High-Tech B.V., The Netherlands) and electro-valves. Since it is well known that higher flow rates lead to greater resistance changes, it is worth noting that the low flow rate applied sacrifices response intensity but has the advantage of enabling lower power consumption and working under more realistic experimental conditions. The effect of the ambient moisture on the sensor's performance was also assessed by using a controller evaporator mixer (Bronkhorst High-Tech B.V., The Netherlands) for humidifying the atmosphere.

The sensor resistances were monitored using a multimeter (HP 34972A, Agilent, USA), registering the resistance changes induced by different concentrations of gases. Specifically, the sensors were exposed to given concentrations of target gases for 5 min and subsequently stabilized for 15 min under dry airflow. Several concentrations of gas species were applied by performing successive dilutions with pure dry air, and the sensing responses were defined as $(\Delta R/R_0)$ expressed in percentage. Where R_0 is defined as the resistance level of the sensor in the air, while ΔR corresponds to the resistance changes obtained over 5 min of gas exposure.

Optical Gas Sensing Measurements. Samples for carrying out UV−vis and PL experiments were prepared by dispersing 5 mg of the sample (Mo_6 or Mo_6@Graphene) in 1 mL of acetonitrile and sonicated for 10 min. Subsequently, the suspensions were deposited by drop-casting on an acid-treated quartz substrate (Mo_6 sample) and an alumina substrate (Mo_6@Graphene sample) placed on a hotplate at 50 °C. Then, the samples were placed inside a screw cap cuvette and fixed with a small piece of commercial Blu-Tack (Figure S17). The samples were purged for 20 min with Ar, air, and NO_2 (balanced with pure synthetic air) before each in situ measurement. The measurements with NH_3 were done by gas diffusion of 10 μL of ammonium hydroxide solution (28% NH_3 wt, Sigma-Aldrich) placed at the bottom of the cuvette. The amount of gaseous NH_3 was calculated from Henry's law (H^{cp} = 0.58 M/Pa at 298.15 K) considering the equilibrium concentration of ammonia in solution ($k_b = 1.8 \times 10^{-5}$).

Stability Studies of the Samples toward Selected Gases. The stability of the nanomaterials was monitored by registering the powder X-ray diffraction patterns and Raman spectra of both nanomaterials (deposited as a thin film on glass substrates) before and after exposure to NO_2 and NH_3 gases. These measurements were

https://doi.org/10.1021/acsami.2c15716
ACS Appl. Mater. Interfaces 2022, 14, 57122−57132

done with 30 min of exposure to each gas in a 5 mL vial with a septum and following a similar methodology as that described in the previous subsection.

Computational Details. The calculations were conducted with the Gaussian 09 program suite. Density functional theory was applied with the PBE0 functional.[62,63] Relativistic electron core potentials from the Stuttgart group and its associated basis sets[64] were used to represent the molybdenum[65] and iodine atoms[66] and augmented in the case of Mo by an f polarization function (Mo/α = 1.043)[67] and in the case of I, with a d polarization function (I/α = 0.289).[68] The 6-31G(d,p) basis set was used to represent the remaining atoms (O, N, and H) of the molecular systems. The geometry optimizations were performed in the gas phase without any symmetry constraint, followed by analytical frequency calculations to confirm that a minimum has been reached. Zero-point energies were included in BE calculations, and the BEs were calculated using BE = $E_{\text{cluster-molecule}} - [E_{\text{cluster}} + E_{\text{molecule}}]$.

The *trans*- and *cis*-$[Mo_6I^i_8(OH)^a_4(H_2O)^a_2]$ isomers were built as representative models for adsorption sites due to the fact that water and hydroxo positioning around the octahedral metal framework cannot be inferred from the X-ray diffraction structure. The guess geometries of the gas−cluster adducts were raised considering a random positioning of the gas analyte with respect to all the cluster ligands (water, hydroxo, and iodide) of the two cluster isomers.

■ ASSOCIATED CONTENT

Supporting Information

The Supporting Information is available free of charge at https://pubs.acs.org/doi/10.1021/acsami.2c15716.

Additional experimental and computational results, including photographs of the device and setups (PDF)

■ AUTHOR INFORMATION

Corresponding Authors

Juan Casanova-Chafer − *MINOS Research Group, Department of Electronics Engineering, Universitat Rovira i Virgili, Tarragona 43007, Spain;* orcid.org/0000-0002-3508-3462; Email: juan.casanova@urv.cat

Marta Feliz − *Instituto de Tecnología Química, Universitat Politècnica de València - Consejo Superior de Investigaciones Científicas (UPV-CSIC), Valencia 46022, Spain;* orcid.org/0000-0002-4429-0551; Email: mfeliz@itq.upv.es

Authors

Rocio Garcia-Aboal − *Instituto de Tecnología Química, Universitat Politècnica de València - Consejo Superior de Investigaciones Científicas (UPV-CSIC), Valencia 46022, Spain*

Pedro Atienzar − *Instituto de Tecnología Química, Universitat Politècnica de València - Consejo Superior de Investigaciones Científicas (UPV-CSIC), Valencia 46022, Spain;* orcid.org/0000-0002-0356-021X

Eduard Llobet − *MINOS Research Group, Department of Electronics Engineering, Universitat Rovira i Virgili, Tarragona 43007, Spain;* orcid.org/0000-0001-6164-4342

Complete contact information is available at: https://pubs.acs.org/10.1021/acsami.2c15716

Author Contributions

J.C.-C., R.G.-A., P.A., M.F., and E.L. conceived and planned the experiments. R.G.-A. and M.F. carried out the cluster synthesis and characterization. J.C.-C. prepared the hybrid and carried out the resistive measurements. R.G.-A. and P.A. carried out the optical measurements. J.C.-C. performed the data analysis. M.F. performed the DFT calculations. M.F and E.L. supervised the work. All the authors wrote the manuscript. All the authors provided critical feedback and helped shape the research. All the authors have given approval to the final version of the manuscript.

Funding

J.C.-C. gratefully thanks ICREA Academia (project: 2018 ICREA Academia-01-AJUT). This research was funded from project PID2021-123163OB-I00 funded by MCIN/AEI/10.13039/501100011033/ and FEDER A way of making Europe, and Generalitat Valenciana (grant number AICO/2020/149). This work was partially funded by MICINN and FEDER via grant no. RTI2018-101580-B-I00. E. L. was supported by the Catalan Institution for Research and Advanced Studies via the 2018 Edition of the ICREA Academia Award.

Notes

The authors declare no competing financial interest.

■ ACKNOWLEDGMENTS

The authors gratefully acknowledge Ana Moreno for her assistance during the cluster synthesis. The technical staff at ITQ and the Electron Microscopy Service at UPV are also acknowledged for their help in sample characterization.

■ REFERENCES

(1) Landrigan, P. J. Air Pollution and Health. *Lancet Public Health* **2017**, *2*, e4−e5.

(2) Song, Z.; Ye, W.; Chen, Z.; Chen, Z.; Li, M.; Tang, W.; Wang, C.; Wan, Z.; Poddar, S.; Wen, X.; Pan, X.; Lin, Y.; Zhou, Q.; Fan, Z. Wireless Self-Powered High-Performance Integrated Nanostructured-Gas-Sensor Network for Future Smart Homes. *ACS Nano* **2021**, *15*, 7659−7667.

(3) Ollé, E. P.; Farré-Lladós, J.; Casals-Terré, J. Advancements in Microfabricated Gas Sensors and Microanalytical Tools for the Sensitive and Selective Detection of Odors. *Sensors* **2020**, *20*, 5478.

(4) Dey, A. Semiconductor Metal Oxide Gas Sensors: A Review. *Mater. Sci. Eng. B* **2018**, *229*, 206−217.

(5) Ratinac, K. R.; Yang, W.; Ringer, S. P.; Braet, F. Toward Ubiquitous Environmental Gas Sensors-Capitalizing on the Promise of Graphene. *Environ. Sci. Technol.* **2010**, *44*, 1167−1176.

(6) Stanford, M. G.; Yang, K.; Chyan, Y.; Kittrell, C.; Tour, J. M. Laser-Induced Graphene for Flexible and Embeddable Gas Sensors. *ACS Nano* **2019**, *13*, 3474−3482.

(7) Zhao, H.; Fan, S.; Chen, Y.; Feng, Z.; Zhang, H.; Pang, W.; Zhang, D.; Zhang, M. Oxygen Plasma-Treated Graphene Oxide Surface Functionalization for Sensitivity Enhancement of Thin-Film Piezoelectric Acoustic Gas Sensors. *ACS Appl. Mater. Interfaces* **2017**, *9*, 40774−40781.

(8) Wu, Y.; Jia, P.; Xu, L.; Chen, Z.; Xiao, L.; Sun, J.; Zhang, J.; Huang, Y.; Bielawski, C. W.; Geng, J. Tuning the Surface Properties of Graphene Oxide by Surface-Initiated Polymerization of Epoxides: An Efficient Method for Enhancing Gas Separation. *ACS Appl. Mater. Interfaces* **2017**, *9*, 4998−5005.

(9) Lee, K.; Yoo, Y. K.; Chae, M. S.; Hwang, K. S.; Lee, J.; Kim, H.; Hur, D.; Lee, J. H. Highly Selective Reduced Graphene Oxide (RGO) Sensor Based on a Peptide Aptamer Receptor for Detecting Explosives. *Sci. Rep.* **2019**, *9*, 10297.

(10) Ruiz, E.; Gueye, T.; Masson, C.; Varenne, C.; Pauly, A.; Brunet, J.; Ndiaye, A. L. Macrocycle-Functionalized RGO for Gas Sensors for BTX Detection Using a Double Transduction Mode. *Chemosensors* **2021**, *9*, 346.

(11) Behi, S.; Casanova-Chafer, J.; González, E.; Bohli, N.; Llobet, E.; Abdelghani, A. Metal loaded nano-carbon gas sensor array for pollutant detection *. *Nanotechnology* **2022**, *33*, 195501.

(12) Zanolli, Z.; Leghrib, R.; Felten, A.; Pireaux, J. J.; Llobet, E.; Charlier, J. C. Gas Sensing with Au-Decorated Carbon Nanotubes. *ACS Nano* **2011**, *5*, 4592−4599.
(13) Mane, A. A.; Suryawanshi, M. P.; Kim, J. H.; Moholkar, A. V. Highly Selective and Sensitive Response of 30.5 % of Sprayed Molybdenum Trioxide (MoO3) Nanobelts for Nitrogen Dioxide (NO2) Gas Detection. *J. Colloid Interface Sci.* **2016**, *483*, 220−231.
(14) Deokar, G.; Vancsó, P.; Arenal, R.; Ravaux, F.; Casanova-Cháfer, J.; Llobet, E.; Makarova, A.; Vyalikh, D.; Struzzi, C.; Lambin, P.; Jouiad, M.; Colomer, J. F. MoS2 -Carbon Nanotube Hybrid Material Growth and Gas Sensing. *Adv. Mater. Interfaces* **2017**, *4*, 1700801.
(15) Singh, S.; Deb, J.; Sarkar, U.; Sharma, S. MoSe2 Crystalline Nanosheets for Room-Temperature Ammonia Sensing. *ACS Appl. Nano Mater.* **2020**, *3*, 9375−9384.
(16) Pham, T.; Li, G.; Bekyarova, E.; Itkis, M. E.; Mulchandani, A. MoS2-Based Optoelectronic Gas Sensor with Sub-parts-per-billion Limit of NO2 Gas Detection. *ACS Nano* **2019**, *13*, 3196−3205.
(17) Dhara, S.; Jawa, H.; Ghosh, S.; Varghese, A.; Karmakar, D.; Lodha, S. All-Electrical High-Sensitivity, Low-Power Dual-Mode Gas Sensing and Recovery with a WSe2/MoS2 pn Heterodiode. *ACS Appl. Mater. Interfaces* **2021**, *13*, 30785−30796.
(18) Ricciardella, F.; Lee, K.; Stelz, T.; Hartwig, O.; Prechtl, M.; McCrystall, M.; McEvoy, N.; Duesberg, G. S. Calibration of Nonstationary Gas Sensors Based on Two-Dimensional Materials. *ACS Omega* **2020**, *5*, 5959−5963.
(19) Nguyen, N. T. K.; Lebastard, C.; Wilmet, M.; Dumait, N.; Renaud, A.; Cordier, S.; Ohashi, N.; Uchikoshi, T.; Grasset, F. A Review on Functional Nanoarchitectonics Nanocomposites Based on Octahedral Metal Atom Clusters (Nb6, Mo6, Ta6, W6, Re6): Inorganic 0D and 2D Powders and Films. *Sci. Technol. Adv. Mater.* **2022**, *23*, 547−578.
(20) Osborn, D. J.; Baker, G. L.; Ghosh, R. N. Mo6Cl12-Incorporated Sol-Gel for Oxygen Sensing Applications. *J. Sol-Gel Sci. Technol.* **2005**, *36*, 5−10.
(21) Ghosh, R. N.; Askeland, P. A.; Kramer, S.; Loloee, R. Optical Dissolved Oxygen Sensor Utilizing Molybdenum Chloride Cluster Phosphorescence. *Appl. Phys. Lett.* **2011**, *98*, 221103.
(22) Ghosh, R. N.; Baker, G. L.; Ruud, C.; Nocera, D. G. Fiber-Optic Oxygen Sensor Using Molybdenum Chloride Cluster Luminescence. *Appl. Phys. Lett.* **1999**, *75*, 2885.
(23) Amela-Cortes, M.; Paofai, S.; Cordier, S.; Folliot, H.; Molard, Y. Tuned Red NIR Phosphorescence of Polyurethane Hybrid Composites Embedding Metallic Nanoclusters for Oxygen Sensing. *Chem. Commun.* **2015**, *51*, 8177−8180.
(24) Jackson, J. A.; Newsham, M. D.; Worsham, C.; Nocera, D. G. Efficient Singlet Oxygen Generation from Polymers Derivatized with Hexanuclear Molybdenum Clusters. *Chem. Mater.* **1996**, *8*, 558−564.
(25) Muñoz, S.; Alvarado-Soto, L.; Gaete, J.; Morales-Verdejo, C.; Ramírez-Tagle, R. Cluster of Hexamolybdenum [Mo6Cl14]2-for Sensing Nitroaromatic Compounds. *ACS Omega* **2022**, *7*, 19152−19157.
(26) Elistratova, J.; Mikhailov, M.; Burilov, V.; Babaev, V.; Rizvanov, I.; Mustafina, A.; Abramov, P.; Sokolov, M.; Konovalov, A.; Fedin, V. Supramolecular Assemblies of Triblock Copolymers with Hexanuclear Molybdenum Clusters for Sensing Antibiotics in Aqueous Solutions via Energy Transfer. *RSC Adv.* **2014**, *4*, 27922−27930.
(27) Zarate, X.; Schott, E.; Alvarado-Soto, L.; Ramirez-Tagle, R. A family of octahedral molybdenum cluster complexes [Mo6Cl8(H2O)-n(OH)6−n]n−2 with n=0-6 as a pH-sensors: A theoretical study. *Chem. Phys. Lett.* **2013**, *567*, 39−42.
(28) Harada, K.; Nguyen, T. K. N.; Grasset, F.; Comby-Zerbino, C.; MacAleese, L.; Chirot, F.; Dugourd, P.; Dumait, N.; Cordier, S.; Ohashi, N.; Matsuda, M.; Uchikoshi, T. Light-Dependent Ionic-Electronic Conduction in an Amorphous Octahedral Molybdenum Cluster Thin Film. *NPG Asia Mater.* **2022**, *14*, 21.
(29) Puche, M.; García-Aboal, R.; Mikhaylov, M. A.; Sokolov, M. N.; Atienzar, P.; Feliz, M. Enhanced Photocatalytic Activity and Stability in Hydrogen Evolution of Mo6 Iodide Clusters Supported on Graphene Oxide. *Nanomaterials* **2020**, *10*, 1259.
(30) Feliz, M.; Atienzar, P.; Amela-Cortés, M.; Dumait, N.; Lemoine, P.; Molard, Y.; Cordier, S. Supramolecular Anchoring of Octahedral Molybdenum Clusters onto Graphene and Their Synergies in Photocatalytic Water Reduction. *Inorg. Chem.* **2019**, *58*, 15443−15454.
(31) Feliz, M.; Puche, M.; Atienzar, P.; Concepción, P.; Cordier, S.; Molard, Y. In Situ Generation of Active Molybdenum Octahedral Clusters for Photocatalytic Hydrogen Production from Water. *ChemSusChem* **2016**, *9*, 1963−1971.
(32) Kumar, S.; Khatri, O. P.; Cordier, S.; Boukherroub, R.; Jain, S. L. Graphene Oxide Supported Molybdenum Cluster: First Heterogenized Homogeneous Catalyst for the Synthesis of Dimethylcarbonate from CO 2 and Methanol. *Chem.—Eur. J.* **2015**, *21*, 3488−3494.
(33) Kwak, D.; Lei, Y.; Maric, R. Ammonia Gas Sensors: A Comprehensive Review. *Talanta* **2019**, *204*, 713−730.
(34) Schoonover, J. R.; Zietlow, T. C.; Clark, D. L.; Heppert, J. A.; Chisholm, M. H.; Gray, H. B.; Sattelberger, A. P.; Woodruff, W. H. Resonance Raman Spectra of [M6X8Y6]2- Cluster Complexes (M = Mo, W; X, Y = Cl, Br, I). *Inorg. Chem.* **1996**, *35*, 6606−6613.
(35) Zhan, J.; Lei, Z.; Zhang, Y. Non-Covalent Interactions of Graphene Surface: Mechanisms and Applications. *Chem* **2022**, *8*, 947−979.
(36) Georgakilas, V.; Tiwari, J. N.; Kemp, K. C.; Perman, J. A.; Bourlinos, A. B.; Kim, K. S.; Zboril, R. Noncovalent Functionalization of Graphene and Graphene Oxide for Energy Materials, Biosensing, Catalytic, and Biomedical Applications. *Chem. Rev.* **2016**, *116*, 5464−5519.
(37) Casanova-Chafer, J.; Umek, P.; Acosta, S.; Bittencourt, C.; Llobet, E. Graphene Loading with Polypyrrole Nanoparticles for Trace-Level Detection of Ammonia at Room Temperature. *ACS Appl. Mater. Interfaces* **2021**, *13*, 40909−40921.
(38) U.S. Environmental Protection Agency. Clean Air Act Text. https://www.epa.gov/clean-air-act-overview/clean-air-act-text (accessed on May 21, 2022).
(39) European Commission. Directive 2008/50/EC on ambient air quality and cleaner air for Europe. https://eur-lex.europa.eu/legal-content/en/ALL/?uri=CELEX%3A32008L0050 (accessed on May 21, 2022).
(40) Samad, A.; Obando Nuñez, D. R. O.; Solis Castillo, G. C. S.; Laquai, B.; Vogt, U. Effect of Relative Humidity and Air Temperature on the Results Obtained from Low-Cost Gas Sensors for Ambient Air Quality Measurements. *Sensors* **2020**, *20*, 5175.
(41) Sheldon, J. C. 76. Bromo- and Iodo-Molybdenum(II) Compounds. *J. Chem. Soc.* **1962**, *0*, 410−415.
(42) Grasset, F.; Dorson, F.; Cordier, S.; Molard, Y.; Perrin, C.; Marie, A.; Sasaki, T.; Haneda, H.; Bando, Y.; Mortier, M. Water-in-Oil Microemulsion Preparation and Characterization of Cs2-[Mo6X14]@SiO2 Phosphor Nanoparticles Based on Transition Metal Clusters (X = Cl, Br, and I). *Adv. Mater.* **2008**, *20*, 143−148.
(43) Sokolov, M. N.; Mihailov, M. A.; Peresypkina, E. V.; Brylev, K. A.; Kitamura, N.; Fedin, V. P. Highly luminescent complexes [Mo6X8(n-C3F7COO)6]2− (X = Br, I). *Dalt. Trans.* **2011**, *40*, 6375−6377.
(44) Mikhailov, M. A.; Brylev, K. A.; Abramov, P. A.; Sakuda, E.; Akagi, S.; Ito, A.; Kitamura, N.; Sokolov, M. N. Synthetic Tuning of Redox, Spectroscopic, and Photophysical Properties of {Mo6I8}-4+Core Cluster Complexes by Terminal Carboxylate Ligands. *Inorg. Chem.* **2016**, *55*, 8437−8445.
(45) Cordier, S.; Dorson, F.; Grasset, F.; Molard, Y.; Fabre, B.; Haneda, H.; Sasaki, T.; Mortier, M.; Ababou-Girard, S.; Perrin, C. Novel Nanomaterials Based on Inorganic Molybdenum Octahedral Clusters. *J. Cluster Sci.* **2008**, *20*, 9−21.
(46) Kirakci, K.; Kubát, P.; Langmaier, J.; Polívka, T.; Fuciman, M.; Fejfarová, K.; Lang, K. A Comparative Study of the Redox and Excited State Properties of (NBu4N)2[Mo6X14] and (NBu4N)2[Mo6X8-(CF3COO)6] (X = Cl, Br, or I). *Dalt. Trans.* **2013**, *42*, 7224−7232.

(47) Kirakci, K.; Kubát, P.; Dušek, M.; Fejfarová, K.; Šícha, V.; Mosinger, J.; Lang, K. A Highly Luminescent Hexanuclear Molybdenum Cluster - A Promising Candidate toward Photoactive Materials. *Eur. J. Inorg. Chem.* **2012**, *2012*, 3107−3111.
(48) Pineau, N. J.; Kompalla, J. F.; Güntner, A. T.; Pratsinis, S. E. Orthogonal Gas Sensor Arrays by Chemoresistive Material Design. *Microchim. Acta* **2018**, *185*, 563.
(49) Park, J.; Tabata, H. Gas Sensor Array Using a Hybrid Structure Based on Zeolite and Oxide Semiconductors for Multiple Bio-Gas Detection. *ACS Omega* **2021**, *6*, 21284−21293.
(50) Lian, X.; Zhou, Y. J.; Zhang, H. F.; Li, M.; Huang, X. C. Luminescence turn-on detection by an entanglement-protected MOF operating via a divided receptor-transducer protocol. *J. Mater. Chem. C* **2020**, *8*, 3622−3625.
(51) Mirochnik, A. G.; Petrochenkova, N. V.; Shishov, A. S.; Bukvetskii, B. V.; Emelina, T. B.; Sergeev, A. A.; Voznesenskii, S. S. Europium(III) Tris-Dibenzoylmethanate as an Efficient Chemosensor for Detection of Ammonia. *Spectrochim. Acta, Part A* **2016**, *155*, 111−115.
(52) Martínez-Ahumada, E.; Díaz-Ramírez, M. L.; Velásquez-Hernández, M. d. J.; Jancik, V.; Ibarra, I. A. Capture of Toxic Gases in MOFs: SO2, H2S, NH3 and NOx. *Chem. Sci.* **2021**, *12*, 6772−6799.
(53) Rieth, A. J.; Dincă, M. Controlled Gas Uptake in Metal-Organic Frameworks with Record Ammonia Sorption. *J. Am. Chem. Soc.* **2018**, *140*, 3461−3466.
(54) Bünzli, J. C. G.; Piguet, C. Taking Advantage of Luminescent Lanthanide Ions. *Chem. Soc. Rev.* **2005**, *34*, 1048−1077.
(55) Wang, B.; Jiang, W.; Dai, X.; Gao, Y.; Wang, Z.; Zhang, R. Q. Molecular Orbital Analysis of the Hydrogen Bonded Water Dimer. *Sci. Rep.* **2016**, *6*, 22099.
(56) Santra, B.; Michaelides, A.; Scheffler, M. On the Accuracy of Density-Functional Theory Exchange-Correlation Functionals for H Bonds in Small Water Clusters: Benchmarks Approaching the Complete Basis Set Limit. *J. Chem. Phys.* **2007**, *127*, 184104.
(57) Akagi, S.; Fujii, S.; Horiguchi, T.; Kitamura, N. pK a(L) Dependences of Structural, Electrochemical, and Photophysical Properties of Octahedral Hexamolybdenum(II) Clusters: [Mo6 X 8 L 6]2− (X = Br or I; L = carboxylate). *J. Cluster Sci.* **2016**, *28*, 757−772.
(58) Kumar, P. V.; Bernardi, M.; Grossman, J. C. The Impact of Functionalization on the Stability, Work Function, and Photoluminescence of Reduced Graphene Oxide. *ACS Nano* **2013**, *7*, 1638−1645.
(59) Georgakilas, V.; Otyepka, M.; Bourlinos, A. B.; Chandra, V.; Kim, N.; Kemp, K. C.; Hobza, P.; Zboril, R.; Kim, K. S. Functionalization of Graphene: Covalent and Non-Covalent Approaches, Derivatives and Applications. *Chem. Rev.* **2012**, *112*, 6156−6214.
(60) Sullivan, K. T.; Wu, C.; Piekiel, N. W.; Gaskell, K.; Zachariah, M. R. Synthesis and Reactivity of Nano-Ag2O as an Oxidizer for Energetic Systems Yielding Antimicrobial Products. *Combust. Flame* **2013**, *160*, 438−446.
(61) Kirakci, K.; Cordier, S.; Perrin, C. Synthesis and Characterization of Cs2Mo6X14 (X = Br or I) Hexamolybdenum Cluster Halides: Efficient Mo6 Cluster Precursors for Solution Chemistry Syntheses. *Z. Anorg. Allg. Chem.* **2005**, *631*, 411−416.
(62) Perdew, J. P.; Burke, K.; Ernzerhof, M. Generalized Gradient Approximation Made Simple. *Phys. Rev. Lett.* **1996**, *77*, 3865.
(63) Adamo, C.; Barone, V. Toward Reliable Density Functional Methods without Adjustable Parameters: The PBE0 Model. *J. Chem. Phys.* **1999**, *110*, 6158.
(64) Andrae, D.; Häußermann, U.; Dolg, M.; Stoll, H.; Preuß, H. Energy-Adjustedab Initio Pseudopotentials for the Second and Third Row Transition Elements. *Theor. Chim. Acta* **1990**, *77*, 123−141.
(65) Dolg, M.; Wedig, U.; Stoll, H.; Preuss, H. Energy-adjusted Ab Initio Pseudopotentials for the First Row Transition Elements. *J. Chem. Phys.* **1998**, *86*, 866.
(66) Bergner, A.; Dolg, M.; Küchle, W.; Stoll, H.; Preuß, H. Ab initio energy-adjusted pseudopotentials for elements of groups 13-17. *Mol. Phys.* **2006**, *80*, 1431−1441.
(67) Ehlers, A. W.; Böhme, M.; Dapprich, S.; Gobbi, A.; Höllwarth, A.; Jonas, V.; Köhler, K. F.; Stegmann, R.; Veldkamp, A.; Frenking, G. A Set of F-Polarization Functions for Pseudo-Potential Basis Sets of the Transition Metals Sc—Cu, Y—Ag and La—Au. *Chem. Phys. Lett.* **1993**, *208*, 111−114.
(68) Höllwarth, A.; Böhme, M.; Dapprich, S.; Ehlers, A. W.; Gobbi, A.; Jonas, V.; Köhler, K. F.; Stegmann, R.; Veldkamp, A.; Frenking, G. A Set of D-Polarization Functions for Pseudo-Potential Basis Sets of the Main Group Elements Al—Bi and f-Type Polarization Functions for Zn, Cd, Hg. *Chem. Phys. Lett.* **1993**, *208*, 237−240.

https://doi.org/10.1021/acsami.2c15716
ACS Appl. Mater. Interfaces 2022, 14, 57122−57132